

**Deciphering Ni sequestration in soil ferromanganese nodules by combining X-ray  
fluorescence, absorption and diffraction at micrometer scales of resolution**

Alain Manceau<sup>1,2</sup>, Nobumichi Tamura<sup>1</sup>, Matthew A. Marcus<sup>1</sup>, Alastair A. MacDowell<sup>1</sup>, Richard S.  
Celestre<sup>1</sup>, Robert E. Sublett<sup>1</sup>, Garrison Sposito<sup>3</sup> and Howard A. Padmore<sup>1</sup>

<sup>1</sup> Advanced Light Source, Lawrence Berkeley National Laboratory, One Cyclotron Road, Berkeley,  
California 94720, USA

<sup>2</sup> Environmental Geochemistry Group, LGIT, University J. Fourier and CNRS, 38041 Grenoble  
Cedex 9, France

<sup>3</sup> Geochemistry Department, Earth Sciences Division, Lawrence Berkeley National Laboratory,  
University of California, Berkeley, CA 94720, USA

Corresponding author: A. Manceau, E-mail: Alain.Manceau@obs.ujf-grenoble.fr

Key words: SXRF, XRD, EXAFS, ferromanganese nodule, soil, speciation.

## Abstract

X-ray microprobes are among the most important new analytical techniques, which have emerged from 3<sup>rd</sup> generation synchrotron facilities. Here we show how X-ray fluorescence, diffraction, and absorption can be used in parallel to determine the structural form of trace elements in heterogeneous matrices at the micrometer-scale of resolution. Scanning X-ray microfluorescence ( $\mu$ SXRF) and microdiffraction ( $\mu$ SXRD) first are used to identify the host solid phase by mapping the distributions of elements and solid species, respectively. Micro-extended X-ray absorption fine structure ( $\mu$ EXAFS) spectroscopy is then used to determine the mechanism of trace element binding by the host phase at the molecular scale. To illustrate the complementary application of these three techniques, we studied how nickel is sequestered in soil ferromanganese nodules, an overwhelmingly complex natural matrix consisting of submicrometer to nanometer sized particles with varying structures and chemical compositions. We show that nickel substitutes for  $\text{Mn}^{3+}$  in the manganese layer of the  $\text{MnO}_2$ - $\text{Al}(\text{OH})_3$  mixed-layer oxide lithiophorite. The affinity of Ni for lithiophorite was characteristic of micronodules sampled from soils across the USA and Europe. Since many natural and synthetic materials are heterogeneous at nanometer to micrometer scales, the synergistic use of  $\mu$ SXRF,  $\mu$ SXRD, and  $\mu$ EXAFS is expected to have broad applications to earth and materials science.

## Introduction

Environmental materials are intrinsically complex, being chemically and structurally heterogeneous at all scales, and their study poses a challenge for investigating metal speciation using conventional techniques. The main difficulties are the partitioning of trace elements into coexisting mineral phases, the identification of the mineral species to which these elements are bound, and the multiplicity of uptake mechanisms. In the absence of robust analytical techniques that could reliably identify each chemical species and quantify their fraction, operationally-defined chemical extractions have been developed during the last two decades, and several procedures have been certified for quality assurance by the Commission of the European Communities Bureau of Reference (Quevauviller et al., 1994). In these methods, chemical reagents of various strengths are used to break the binding forces and to liberate and subsequently extract the metals from the mineral phases having different stabilities. However, uncertainties remain related to the selectivity of the various extractants and to potential problems due to re-adsorption of the dissolved metal to other phases (Gomez-Ariza and al., 2000; Ho and Evans, 2001; Ostergren et al., 1999). Several physical techniques alternatively are used to investigate the crystal chemistry of trace metal impurities in solids, of which electron microscopy (Buseck, 1992) and bulk extended X-ray absorption fine structure (EXAFS) (Brown et al., 1999; Manceau et al., 2002) are among the most efficient. However, as powerful and often-used as these methods are, none of them, separately or together, allow one to identify both the nature of the host species and the incorporation mechanism of trace metals at the molecular scale. In the most-advanced application of EXAFS spectroscopy to speciation, the number and nature of metal species are rigorously evaluated by principal component analysis (PCA) of a set of experimental spectra. Their proportions subsequently are estimated by least-squares fitting (LSF) of experimental data to the combination of reference spectra previously

identified by PCA. Still, PCA is a wholly statistical analytical treatment of a set of mixed spectra, and the quantification procedure requires that all individual species are present in the reference database. As with any desummation technique, there can be also some concerns about the uniqueness of the analysis. In addition, there is no direct link to the actual solid phases (mineral or organic) present in the sample. X-ray micro-diffraction and micro-fluorescence, as an adjunct to EXAFS spectroscopy, ground this multicomponent spectral analysis in reality, obviating the need for any guesswork. Synchrotron-based scanning X-ray microfluorescence ( $\mu$ SXRF) (Sutton and Rivers, 1999) and microdiffraction ( $\mu$ SXRD) (Tamura et al., 2002) together allow one to visualize the two-dimensional distribution of metals in minerals, and hence to determine to which particular mineral a given metal is bound, by simultaneous imaging of elemental and mineral species distributions within the heterogeneous matrix. The coordination chemistry of the metal, and hence its incorporation mechanism within the mineral host, then is identified by  $\mu$ EXAFS performed on single metal species.

The power of combined fluorescence – diffraction – absorption studies at micrometer-scale resolution is illustrated here by determining how Ni is sequestered in soil ferromanganese nodules. Soils represent a major sink for anthropogenic Ni, and its migration to living organisms is an environmental concern because of its suspected carcinogenicity when it is speciated as nickel sulfate or combinations of nickel sulfides and oxides, provoking lung and nasal cancers (Nriagu, 1980; Yaman, 2000). The anthropogenic nickel sources are metal processing operations, combustion of coal and oil, and amendments by sewage sludge. The crystal chemistry of nickel in oxidized and silicated ores has been studied abundantly for economic reasons, and in these formations Ni is predominantly associated with phyllosilicates and the Fe oxyhydroxide, goethite ( $\alpha$ -FeOOH). During its journey from the source to its resting place in soils, Ni can undergo many chemical transformations, and understanding how this element is naturally sequestered helps

provide a solid scientific basis for maintaining soil quality and formulating educated strategies to remediate severely impacted areas. The most efficient and durable process responsible for trace metal sequestration in soils is the formation of ferromanganese micronodules, which often have been compared to the well-known oceanic Mn nodules (Glasby et al., 1979; Han et al., 2001; White and Dixon, 1996). Although soil micronodules are the premier reservoir for trace metals in soils, the crystal chemistry of the sequestered elements remains poorly understood (Manceau et al., 2002). Nickel is of special interest because chemical analyses of individual nodules from Sicilia and New Zealand showed that this element is enriched in these concretions relative to the soil matrix (Childs, 1975; Palumbo et al., 2001). The micronodules studied here were collected in the plowed layer of agricultural fields of the Morvan region (France) used for livestock breeding activities (Baize and Chrétien, 1994; Latrille et al., 2001). Soils in this area are developed on the Sinemurian calcareous geological setting, and contain 5 - 12 weight percent of ferromanganese pellets termed 'shot', 'lead shot', or 'buckshot' by agriculturists (Baize and Chrétien, 1994; Wheeting, 1936). The nodules are enriched in most trace metals ( $[\text{Ni}] = 534$  ( $\sigma = 99$ ),  $[\text{Zn}] = 4063$  ( $\sigma = 1393$ ),  $[\text{Pb}] = 1423$  ( $\sigma = 1234$ ) mg/Kg; Latrille et al., 2001), but fixed in a form which makes them highly immobile and thus not very accessible to living organisms (i.e., not harmful).

### **Experimental Method**

X-ray diffraction patterns and fluorescence spectra were recorded at fixed energy on Beamline 7.3.3. at the Advanced Light Source (ALS, Berkeley), and then fluorescence X-ray absorption spectra were collected at Beamline 10.3.2 by varying the energy of the incident beam (MacDowell et al., 2001; Padmore et al., 1996) (Fig. 1). On both beamlines, the source is first imaged at 1:1 magnification with a toroidal mirror to a maximum spot size of  $240 \times 35 \mu\text{m}$ , determined by the

source size. This “virtual source” is then imaged by two elliptically bent mirrors, arranged in the Kirkpatrick-Baez (KB) crossed configuration (Kirkpatrick and Baez, 1948). The demagnification of this mirror pair is 28.3 horizontal (H) x 12.5 vertical (V) (7.3.3) and 20 (H) x 6 (V) (10.3.2). The spot size on the sample is adjusted with slits placed at the virtual source to trade flux for lateral resolution. The divergence of the beam after the KB mirrors is 3.7 x 1.6 mrad (7.3.3) or 4.1 x 1.7 mrad (10.3.2). For micro-spectroscopy (10.3.2), an additional parabola mirror collimates the incoming beam in the vertical direction to match the vertical divergence of the beam to the acceptance of the monochromator. On both stations, the monochromator consists of two channel cut Si(111) crystals mounted in a dispersive arrangement such that wavelength scanning is accomplished by rotating the crystal pairs in opposite directions. This system has proven highly stable; in practice, rocking of the 2<sup>nd</sup> crystal to track the reflection of the 1<sup>st</sup> crystal pair is unnecessary. With this geometry, the beam remains stable in position on the sample while scanning in energy. This is very important for the recording of  $\mu$ EXAFS data, where drifts of the beam on and off the micron-sized sample of interest would result in signal variations, which could mimic features of EXAFS spectra.

The distribution of nanometer-sized particles, which are the most reactive towards metal sorption, was imaged at a resolution of 20 x 20  $\mu$ m by collecting point powder XRD patterns and integrating the diffracted intensity along the Debye rings of X-rays. XRD patterns were conveniently measured alongside fluorescence spectra using a large area CCD camera (Bruker 6000, active area of 9 x 9 cm) placed above the specimen stage (Fig. 1a). Samples were prepared as 30  $\mu$ m-thick micropolished thin sections adhered to glass slides and inclined at 6° to the horizontal plane. At this angle, the lateral size of the illuminated area was 14  $\mu$ m (H) x 11  $\mu$ m (V). In principle, diffraction may be collected in transmission with photon energies of about 10-12 keV, but in practice the best results were obtained by recording diffraction in reflection with an excitation

energy (6.3 keV) below the absorption edge of transition metals present in the matrix (Mn, Fe, Ni, Zn). This arises because at higher energy the fluorescence signal from Mn and Fe enters the detector, thereby adding to the background noise of the diffraction patterns. The distance between the analyzed spot on the sample and CCD, and the  $2\theta$  scale were precisely calibrated using the reflection peaks of quartz grains contained in the sample. Fluorescence maps were obtained by scanning the sample stage under the monochromatic beam at  $E = 10$  keV with a step size of  $20 \times 20$   $\mu\text{m}$ , while recording the X-ray fluorescence with a Ge solid-state detector. Fluorescence-yield nickel K-edge  $\mu\text{EXAFS}$  spectra were then collected on single metal species aggregates at  $16 \mu\text{m H} \times 5 \mu\text{m V}$  resolution. Measurements were carried out by orienting the sample vertically to  $45^\circ$  to both the X-ray beam and the solid-state detector (Fig. 1b).  $\mu\text{SXRF}$  maps were also recorded in this geometry to re-image the areas previously identified by  $\mu\text{SXRD} - \mu\text{SXRF}$ .

## Results and Discussion

Figure 2 illustrates how laterally resolved  $\mu\text{SXRF}$  and  $\mu\text{SXRD}$  data can be used to identify the partitioning of trace elements among coexisting mineral phases within their natural matrix. With  $\mu\text{SXRF}$  the distribution of Fe, Mn, and Ni were determined, and it was found that Mn and Ni were systematically associated in the six different soil nodules examined in this study. Two-dimensional XRD patterns were characterized by the presence of point diffraction spots from sub-micron crystals, including quartz, feldspars, titanium oxides, illite and kaolinite, and continuous Debye rings arising from nanometer-sized particles, including phyllosilicate, goethite ( $\alpha\text{-FeOOH}$ ), and three Mn oxides, lithiophorite, birnessite, and Fe-vernadite (Fig. 2). The mineral abundance maps of the first four finely divided (nanometer-sized) species were produced by integrating at each point-of-analysis the diffracted intensities of the non-overlapping (020) and (200) reflections at  $\sim 4.45$   $\text{\AA}$

and  $\sim 2.57$  Å for phyllosilicate, the (101) and (301) reflections at 4.19 Å and 2.69 Å for goethite, the (001) reflection at 7.1-7.2 Å for birnessite, and the (001) and (002) reflections at 9.39 Å and 4.69 Å for lithiophorite. Kaolinite and illite grains have intense reflection maxima at 7.14 Å, and  $\sim 4.46$  Å and  $\sim 2.57$  Å, respectively, which overlap with reflections from birnessite and nanometer-sized phyllosilicate particles (smectitic clays). This difficulty in the mineralogical analysis of soils is well-known and has often prevented the unambiguous identification of these minerals by conventional XRD analysis (Rhoton et al., 1993; Taylor et al., 1964; Tokashiki et al., 1986). Since kaolinite and illite grains are comparable in size to the X-ray beam, they yield strongly textured two-dimensional  $\mu$ XRD patterns, which contrast with the powder XRD patterns from minute particles, hence allowing one to separate analytically the two kind of patterns in two-dimensional  $\mu$ XRD experiments. The reliability of this quantitative treatment was verified by comparing mineral maps calculated using independent (*hkl*) reflections of the same mineral species. The distribution of Fe-vernadite, a common soil mineral (Chukhrov and Gorshkov, 1981; Vodyanitskii et al., 2001), was not mapped because it was systematically detected throughout the examined nodules without any significant concentration gradient. This Fe-Mn disordered phase (also termed Mn-feroxyhite), which is dispersed throughout the nodule matrix filling pores and aggregating coarse grains, acts as a cementing agent for the nodules. The comparison of the  $\mu$ SXRF and  $\mu$ SXRD maps clearly shows that nickel and lithiophorite have the same contour maps, therefore suggesting that Ni is bound to this particular mineral phase. However, it should be noted that an association between an element *E* and a mineral *M* does not necessarily imply that *E* is chemically bound to or included in the structure of *M*. Still, we shall see, however, from the EXAFS that Ni is indeed included in the lithiophorite structure. We note that this nodule contains regions in which birnessite and lithiophorite coexist, therefore, the recording of point- $\mu$ XRD patterns in these regions would not be conclusive regarding the partitioning of nickel between these two minerals. This finding

demonstrates the usefulness of combining element and mineral maps, and shows that pertinent information can be obtained on nanometer-sized environmental particles at the micrometer-scale of resolution because of their segregation in localized areas. In this case, the heterogeneity of environmental samples becomes an advantage. That goethite is devoid of nickel is also clearly apparent from these maps, which show that the goethite “crown” area contains no nickel.

The systematic association of Ni with lithiophorite suggests that Ni should be located in a definite cation site of the manganese oxide crystal structure. Lithiophorite has a layered structure consisting of alternating  $\text{MnO}_2$  and  $\text{Al}(\text{OH})_3$  octahedral layers, in which, ideally, all Mn sites are occupied and one third of Al sites are empty or occupied by Li (dioctahedral structure, Fig. 3). Phyllosilicates are however rarely stoichiometric, and can accommodate big aliovalent cations ( $\text{Li}^+$ ,  $\text{Ni}^{2+}$ ,  $\text{Cu}^{2+}$ ,  $\text{Zn}^{2+}$ ) in the vacant Al sites, and  $\text{Mn}^{3+}$  ions in  $\text{Mn}^{4+}$  sites. For electrostatic reasons, the resulting positive net charge of the  $\text{Al}(\text{OH})_3$  layer and the negative net charge of the  $\text{MnO}_2$  layer contribute to increase the stability of the mixed-layer framework by increasing the strength of H-bonds. To determine the exact Ni site, Ni K-edge  $\mu\text{EXAFS}$  spectra were collected in Ni-rich regions from several nodules. All spectra were identical, indicating that the incorporation mechanism of Ni is unique, and is the key to understanding its sequestration in soils. Qualitative information about the local structure of Ni can be obtained by comparing the unknown  $\mu\text{EXAFS}$  spectrum to reference EXAFS spectra from relevant model compounds. As expected from  $\mu\text{SXRF}$  –  $\mu\text{SXRD}$  experiments, the two reference spectra for Ni in goethite (Manceau et al., 2000) and phyllosilicate (Manceau and Calas, 1986) did not match the unknown spectrum, confirming that Ni is not sequestered in these forms (data not shown). Differences in frequency and shape of the EXAFS oscillations were also observed with birnessite, in which Ni is sorbed above vacant Mn sites, and with lithiophorite, in which Ni is located within the gibbsitic Al layer (Manceau et al., 1987) (Fig. 4a). Figure 4a shows that despite the arguments given above for assigning the Ni

sorption site to lithiophorite, the EXAFS pattern observed in the soil does not agree with that from the reference sample of Ni in lithiophorite. However, that reference represents one possible mode of incorporation for Ni in this mineral, in which the Ni is in the gibbsitic  $\text{Al}(\text{OH})_3$  layer. We shall now show that we can account for the observed spectrum by assuming another position for the Ni in lithiophorite.

The radial structure functions (RSFs) obtained by Fourier transforming EXAFS spectra for the reference and the soil lithiophorite both exhibit, after the first oxygen peak, a second peak at roughly  $R + \Delta R = 2.6 \text{ \AA}$ , that is at a distance characteristic of edge-sharing linkage between metal octahedra (Fig. 4b). This result alone suggests that Ni is located within one of the two octahedral layers of the lithiophorite structure. To solve this issue, suffice it to examine the phase of the imaginary part of the Fourier transform, because waves backscattered by Al and Mn atoms are almost out-of-phase (Teo, 1986). Examination of Fig. 4b shows that the unknown and lithiophorite reference have their electronic waves shifted by  $\sim\pi$  in the  $2.2 - 3.1 \text{ \AA}$   $R + \Delta R$  interval, thus indicating that Ni is substituted for Mn in the soil lithiophorite. In keeping with this conclusion, the two waves are logically in phase in the  $1.0 - 2.2 \text{ \AA}$   $R + \Delta R$  interval, since in both structures Ni is octahedrally coordinated to oxygen atoms. Crystallographic distances obtained by least-squares fitting experimental data with the WINXAS program (Ressler, 1998) and using amplitude and phase shift functions calculated with FEFF (Rehr et al., 1991), were  $d(\text{Ni-O}) = 2.05 \text{ \AA}$ ,  $d(\text{Ni-Mn}) = 2.91 \text{ \AA}$ ,  $d(\text{Mn-O}) = 1.92 \text{ \AA}$ , and  $d(\text{Mn-Mn}) = 2.92 \text{ \AA}$ . There was no indication of Ni-Ni pairs, for which Ni-Ni distances of  $3.03 \text{ \AA}$  to  $3.12 \text{ \AA}$  would be predicted (Manceau et al., 2000). This result indicates that nickel did not precipitate as a hydroxide, hence confirming that the next-nearest coordination shell of Ni is made of Mn atoms.

Since  $\text{Ni}^{2+}$  has an effective radius 30% greater than that of  $\text{Mn}^{4+}$  (Shannon, 1976), one may wonder how the Ni-Mn substitution is realized. To answer this question, Ni- and Mn-RSFs were

plotted together (Fig. 4c), and the Ni- and Mn-EXAFS interatomic distances compared. A distinct feature in the Ni-RSF is the shift to higher  $R + \Delta R$  values of the Ni-O peak, indicative of a relaxation of the Ni site owing to the larger ion size of the  $\text{Ni}^{2+}$  impurity ( $r = 0.69 \text{ \AA}$ ) relative to  $\text{Mn}^{4+}$  ( $r = 0.53 \text{ \AA}$ ) and  $\text{Mn}^{3+}$  ( $r = 0.645 \text{ \AA}$ ). Since  $\text{Ni}^{2+}$  and  $\text{Mn}^{3+}$  have a size mismatch of only 7%, nickel likely substitutes on the trivalent manganese site. Likewise, the  $\text{Al}^{3+}$  site of the gibbsitic layer is clearly too small ( $r = 0.535 \text{ \AA}$ ) to accommodate  $\text{Ni}^{2+}$ , and the larger  $\text{Li}^+$  site ( $r = 0.76 \text{ \AA}$ ) is probably energetically less favorable. This assumption is supported by recent atomistic calculations and EXAFS measurements on lanthanide-doped perovskite, which showed that the rare earth is energetically stabilized in smaller crystallographic sites (Davies et al., 2000). The same results were obtained on nodules from flood plain soils in the USA, which suggests that the Ni species identified herein may correspond to a major sequestration form of Ni in Earth near-surface environments.

### Acknowledgements

The nodule samples were kindly provided by D. Baize from INRA, France. The ALS is thanked for the provision of beamtime. AM is grateful to LBNL for financial support from the Laboratory Directed Research and Development Program. This work was partly supported by the Director, Office of Energy Research, Office of Basic Energy Sciences, Materials Sciences Division of the U.S. Department of Energy, under Contract No. DE-AC03-76SF00098.

## References

- Baize, D., and Chrétien, J. (1994) Les couvertures pédologiques de la plate-forme sinémurienne en Bourgogne: particularités morphologiques et pédo-géochimiques. *Etude et Gestion des Sols*, 2, 7-27.
- Brown, G.E., Foster, A.L., and Ostergren, J.D. (1999) Mineral surfaces and bioavailability of heavy metals: A molecular-scale perspective. *Proceedings of the National Academy of Sciences, USA*, 96, 3388-3395.
- Buseck, P.R. (1992) Minerals and reactions at the atomic scale: Transmission electron microscopy. Mineralogical Society of America, Washington, D.C.
- Childs, C.W. (1975) Composition of iron-manganese concretions from some New Zealand soils. *Geoderma*, 13, 141-152.
- Chukhrov, F.V. and Gorshkov, A.I. (1981) Iron and manganese oxide minerals in soils. *Transactions of the Royal Society, Edinburgh*, 72, 195-200.
- Davies, R.A., Islam, M.S., Chadwick, A.V., and Rush, G.E. (2000) Cation dopant sites in the CaZrO<sub>3</sub> proton conductor: a combined EXAFS and computer simulation study. *Solid State Ionics*, 130, 115-122.
- Glasby, G.P., Rankin, P.C., and Meylan, M.A. (1979) Manganiferous soil concretions from Hawaii. *Pacific Science*, 33, 103-115.
- Gomez-Ariza, J.L., Giraldez, I., Sanchez-Rodas, D., and Morales, E. (2000) Selectivity assessment of a sequential extraction procedure for metal mobility characterization using model phases. *Talanta*, 52, 545-554.
- Han, F.X., Banin, A., and Triplett, G.B. (2001) Redistribution of heavy metals in arid-zone soils under a wetting-drying cycle soil moisture regime. *Soil Science*, 166, 18-28.

- Ho, M.D., and Evans, G.J. (2001) Sequential extraction of metal contaminated soils with radiochemical assessment of readsorption effects. *Environmental Science and Technology*, 34, 1030-1035.
- Kirkpatrick, P., and Baez, A.V. (1948) Formation of optical images by X-rays. *Journal of the Optical Society of America*, 38, 766-772.
- Latrille, C., Elsass, F., van Oort, F., and Denaix, L. (2001) Physical speciation of trace metals in Fe-Mn concretions from a rendzic lithosol developed on Sinemurian limestones (France). *Geoderma*, 100, 127-146.
- MacDowell, A.A., Celestre, R.S., Tamura, N., Spolenak, R., Valek, B.C., Brown, W.L., Brawman, J.C., Padmore, H.A., Batterman, B.W., and Patel, J.R. (2001) Submicron X-ray diffraction. *Nuclear Instrument and Method, A* 468, 936-943.
- Manceau, A., and Calas, G. (1986) Ni-bearing clay minerals. 2. X-ray absorption study of Ni-Mg distribution. *Clay Minerals*, 21, 341-360.
- Manceau, A., Llorca, S., and Calas, G. (1987) Crystal chemistry of cobalt and nickel in lithiophorite and asbolane from New Caledonia. *Geochimica et Cosmochimica Acta*, 51, 105-113.
- Manceau, A., Schlegel, M.L., Musso, M., Sole, V.A., Gauthier, C., Petit, P.E., and Trolard, F. (2000) Crystal chemistry of trace elements in natural and synthetic goethite. *Geochimica et Cosmochimica Acta*, 64, 3643-3661.
- Manceau, A., Tamura, N., Celestre, R.S., MacDowell, A.A., Sposito G., and Padmore H.A. (2002) Molecular-scale speciation of metals in soils. Submitted.
- Nriagu, J.O. (1980) *Nickel in the Environment*. Wiley, New York.
- Ostergren, J.D., Brown, G.E., Parks, G.A., and Tingle, T.N. (1999) Quantitative lead speciation in selected mine tailings from Leadville, CO. *Environmental Science and Technology*, 33, 1627-1636.

- Padmore, H.A., Howells, M.R., Irick, S., Renner, T., Sandler, R., and Koo, Y.M. (1996) Some new schemes for achieving high-accuracy elliptical x-ray mirrors by elastic bending. *Society of Photo-Optical Instrumentation Engineers (SPIE)*, 2856, 145-156.
- Palumbo, B., Bellanca, A., Neri, R., and Roe, M.J. (2001) Trace metal partitioning in Fe-Mn nodules from Sicilian soils, Italy. *Chemical Geology*, 173, 257-269.
- Quevauviller, P., Rauret, G., Muntau, H., Ure, A.M., Rubio, R., Lopez Sanchez, J.F., Fiedler, H.D., and Griepink, B. (1994) Evaluation of a sequential extraction procedure for the determination of extractable trace metal contents in sediments. *Fresenius Journal of Analytical Chemistry*, 349, 808-814.
- Rehr, J.J., Mustre de Leon, J., Zabinsky, S.I., and Albers, R.C. (1991) Theoretical X-ray Absorption Fine Structure Standards. *Journal of the American Chemical Society*, 113, 5135-5145.
- Ressler, T. (1998) WinXAS: a Program for X-ray Absorption Spectroscopy Data Analysis under MS-Windows. *Journal of Synchrotron Radiation*, 5, 118-122.
- Rhoton, F.E., Bigham, J.M., and Schulze, D.G. (1993) Properties of iron-manganese nodules from a sequence of eroded fragipan soils. *Soil Science Society America Journal*, 57, 1386-1392.
- Shannon, R.D. (1976) Revised effective ionic radius and systematic studies of interatomic distances in halides and chalcogenides. *Acta Crystallographica*, B25, 925-946.
- Sutton, S.R., and Rivers, M.L. (1999) Hard X-ray synchrotron microprobe techniques and applications. In D. Schulze, P. Bertsch, and J. Stucki, Eds. *Synchrotron X-ray Methods in Clay Science*, p. 146-163. Clay Mineral Society of America.
- Tamura, N., Spolenak, R., Valek, B.C., Manceau, A., Meier Chang, N., Celestre, R.S., MacDowell, A.A., Padmore, H.A., and Patel, J.R. (2002) Submicron X-ray diffraction and its applications to problems in materials and environmental science. *Nuclear Instruments and Methods in Physics Research*, in press.

- Taylor, R.M., McKenzie, R.M., and Norrish, K. (1964) The mineralogy and chemistry of manganese in some Australian soils. *Australian Journal of Soil Research*, 2, 235-248.
- Teo, B.K. (1986) EXAFS: basic principles and data analysis. 349 p. Springer-Verlag, Berlin.
- Tokashiki, Y., Dixon, J.B., and Golden, D.C. (1986) Manganese oxide analysis in soils by combined X-ray diffraction and selective dissolution methods. *Soil Science Society America Journal*, 50, 1079-1084.
- Vodyanitskii, Y.N., Lesovaya, S.N., and Sivtsov, A.V. (2001) Iron minerals in soils on red-colored deposits. *Eurasian Soil Science*, 34, 774-782.
- Wheeting, L.C. (1936) Shot soils of Western Washington. *Soil Science*, 41, 35-45.
- White, G.N., and Dixon, J.B. (1996) Iron and manganese distribution in nodules from a young Texas vertisol. *Soil Sci. Soc. Amer. J.*, 60, 1254-1262.
- Yaman, M. (2000) Nickel speciation in soil and the relationship with its concentration in fruits. *Bulletin of Environmental Contamination and Toxicology*, 65, 545-552.

**FIGURE CAPTION**

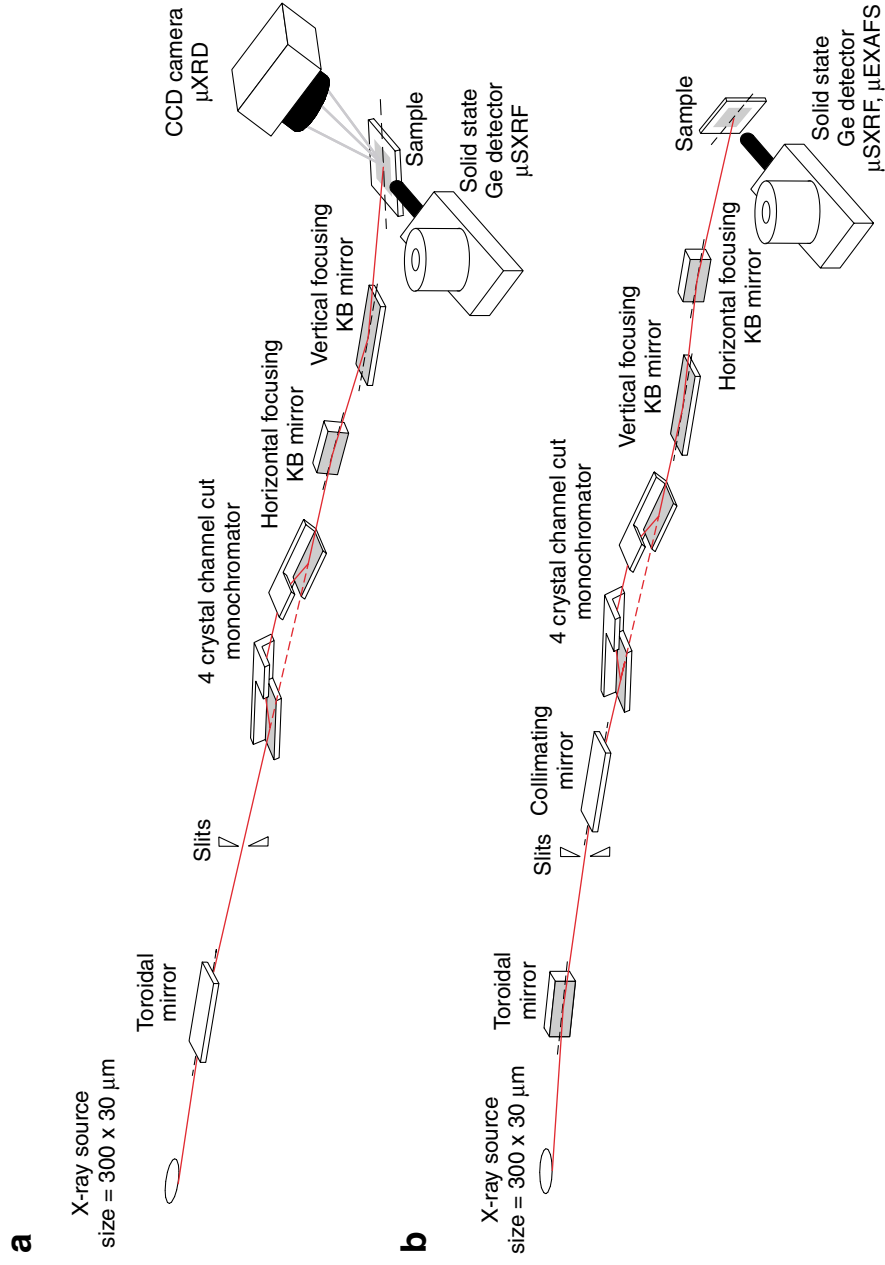
**Figure 1** Schematic diagram of the experimental setups used on stations 7.3.3. (a) and 10.3.2. (b) of the ALS for combined X-ray fluorescence and diffraction (a), and X-ray fluorescence and absorption (b) measurements (MacDowell et al., 2001; Padmore et al., 1996).

**Figure 2** Combined fluorescence - diffraction measurements recorded on a ferromanganese soil nodule (sample TN4 from Baize and Chrétien (1994) and Latrille et al. (2001)). The three images on the top are elemental maps obtained by  $\mu$ SXRF, and the four images on the bottom are mineral species maps obtained by integrating at each point of analysis the intensities of the relevant (*hkl*) reflections along the Debye rings of the two-dimensional XRD patterns (d-spacings are indicated in parenthesis). One XRD pattern is presented to the top right. Li = lithiophorite, Bi = birnessite, P = phyllosilicate, Q = quartz.

**Figure 3** Structure of lithiophorite and incorporation mechanism of nickel in the reference and soil lithiophorite specimen.

**Figure 4** Ni K-edge  $\mu$ EXAFS spectrum (a) and Fourier transform (modulus plus imaginary part) (b, c) from a 'hot spot' of the core of the nodule, compared to the Ni- and Mn-edge data from a Ni-containing lithiophorite reference, in which Ni substitutes for Li in the  $\text{Al}(\text{OH})_3$  layer (Manceau et al., 1987). The peaks in the Fourier transforms are not at their exact expected positions (R values) because of phase-shift effects ( $\Delta R$ ) and disorder arising from the accommodation of atoms having different radii. The Ni-Mn and Mn-Mn contributions at  $R + \Delta R = 2.5 \text{ \AA}$  in c) are almost superimposed (both the modulus and imaginary parts), indicating that the cationic environment of

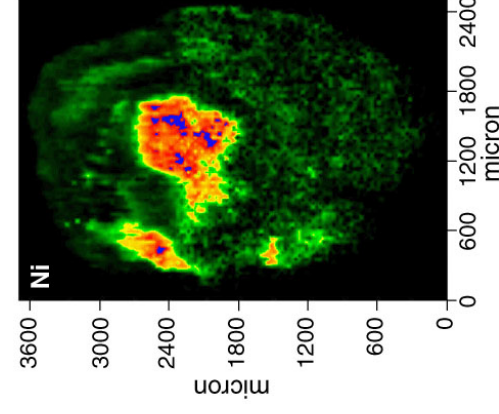
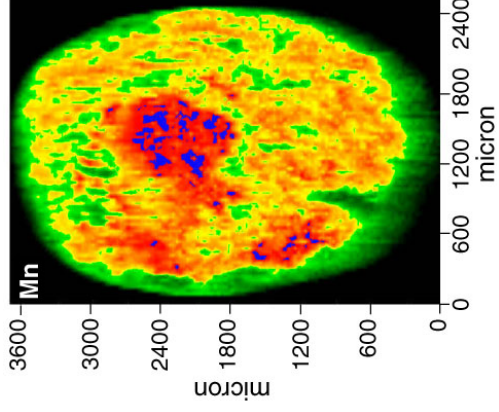
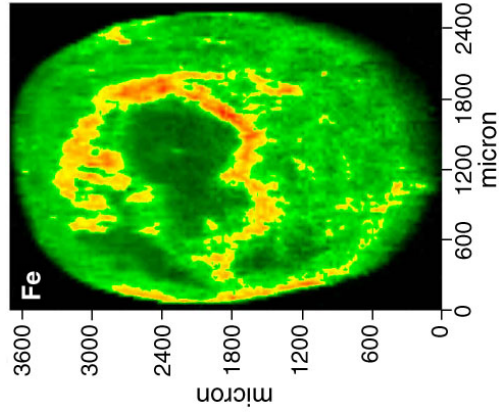
Ni is akin to that of Mn. This is strong evidence that Ni is present at the Mn site in the lithiophorite structure.



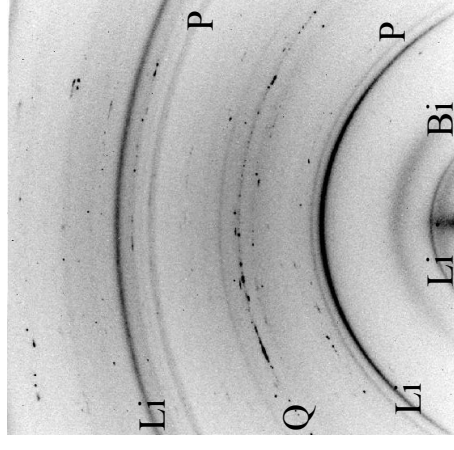
Please, print on two-column format

Fig. 1

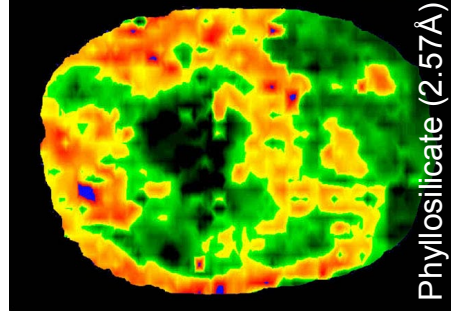
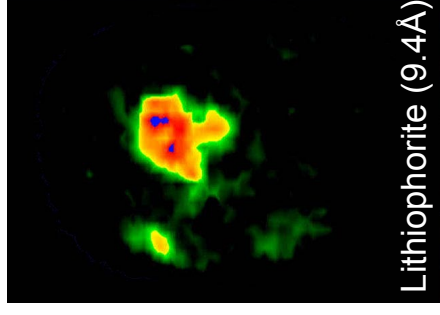
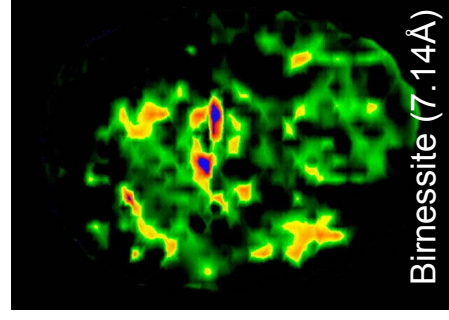
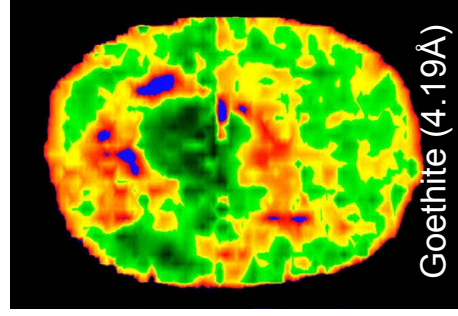
Elemental map ( $\mu$ SXRF)



$\mu$ SXRD pattern

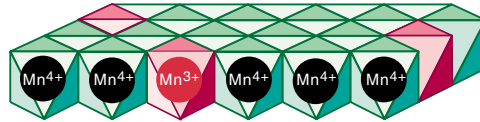


Mineral species map ( $\mu$ SXRD)



Please, print on two-column format Fig. 2

Lithiophorite reference



Soil lithiophorite

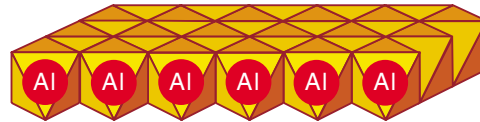
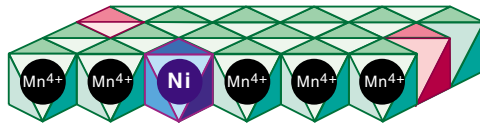


Fig. 3

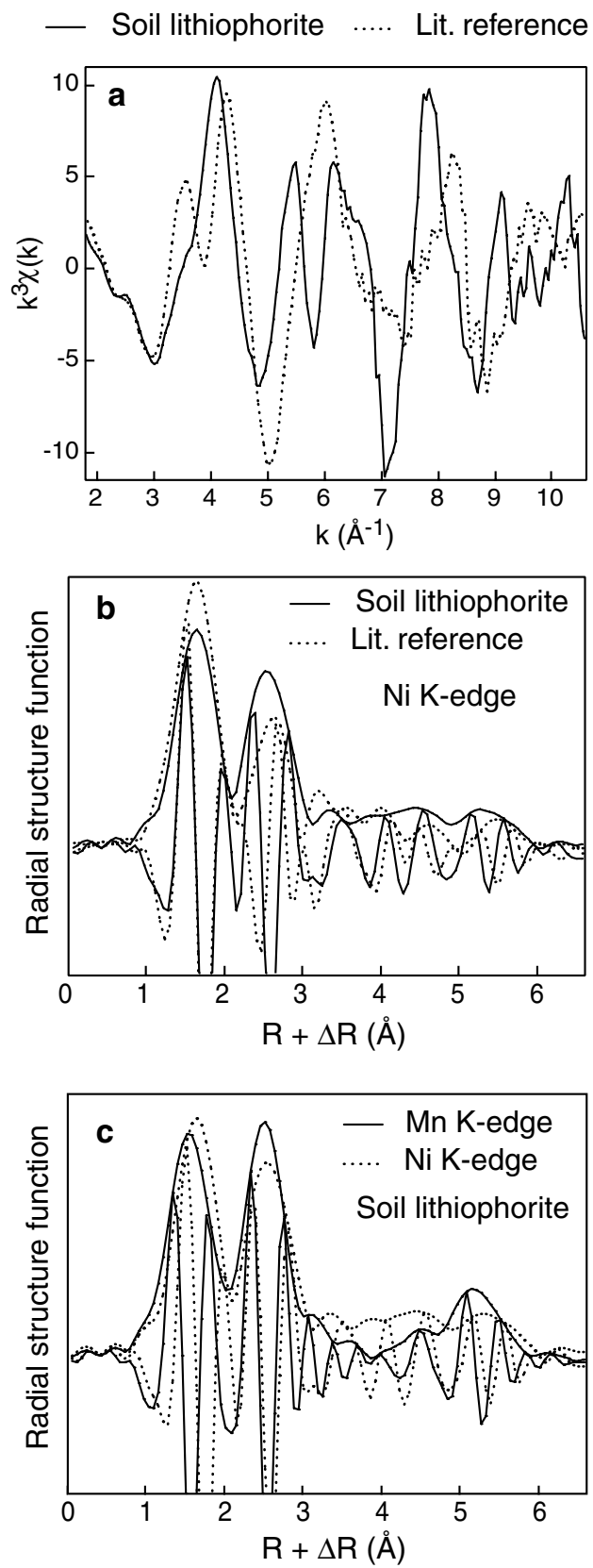


Fig. 4